Zhang, S., Harris, P., Doufexi, A., Nix, A., & Beach, M. (2016). Massive MIMO real-time channel measurements and theoretic TDD downlink throughput predictions. In 2016 IEEE 27th Annual International Symposium on Personal, Indoor, and Mobile Radio Communications (PIMRC). (Personal, Indoor, and Mobile Radio Communications (PIMRC)). Institute of Electrical and Electronics Engineers (IEEE). DOI: 10.1109/PIMRC.2016.7794647

Massive MIMO Real-Time Channel Measurements and Theoretic TDD Downlink Throughput Predictions

Siming Zhang, Paul Harris, Angela Doufexi, Andrew Nix and Mark Beach

Communication Systems & Networks Group, University of Bristol, United Kingdom
{sz1659; paul.harris; A.Doufexi; Andy.Nix; M.A.Beach}@bristol.ac.uk

***Abstract*—This paper is the first to evaluate the realistic performance of Massive MIMO using real-time channel measurements conducted at 3.51GHz. Our testbed consists of 64 National Instruments Universal Software Radio Peripheral Reconfigurable Input and Output (NI USRP RIO) software defined radios (SDRs) with 128 dipole antennas at the Base Station (BS) side, and 6 USRPs configured as 12 single-antenna User Equipment (UE) nodes. The system operates in a Time Division Duplex (TDD) fashion with a Long Term Evolution (LTE) like Physical Layer framework which, when fully deployed, will enable instantaneous throughput measurements on the Uplink (UL) and Downlink (DL) according to a user-defined frame schedule. In this paper we present real-time UL channel measurements at all BS antenna ports simultaneously, which allows the temporal characteristics of the Massive MIMO channel to be recorded. Eigen-beamforming precoding and a Received Bit-level Mutual Information Rate (RBIR) abstraction simulator are then used to predict the theoretic DL performance. We quantify the co-located Massive MIMO throughput for differing numbers of BS antennas (i.e. 32, 64 and 112 elements) and UE locations for an indoor environment.**

Keywords—Massive MU-MIMO, Testbed, Real-time Indoor Channel Measurement, Theoretic Throughput.

I. INTRODUCTION

Massive Multiple-Input-Multiple-Output (MIMO) is one of the key technologies in 5G, and it is envisaged to have superior spectral and energy efficiencies by deploying hundreds of antennas and Radio Frequency (RF) chains at the base station (BS) and simultaneously serving tens of User Equipment (UE) nodes. The theoretical benefits of Massive MIMO have been discussed and presented in many papers such as [1], [2] and [3]. Firstly, the large antenna array gain enhances the received signal power, thus providing improved data rates and cell coverage. Secondly, the powerful beamforming and extra degrees of freedom (DoF) that come from having so many antennas at the basestation allow for not only improved Multi-User (MU) multiplexing gain, but also diversity gain, whereas in traditional Long Term Evolution (LTE) systems, usually there is a trade-off between multiplexing and diversity gains. These gains arise because the BS array can focus into ever-smaller regions of space to transmit and receive signal energy, effectively making the MU-MIMO channel asymptotically orthogonal. Thirdly, the hope for improved energy efficiency lies in the use of inexpensive low-power RF components, bringing the deployment cost down. However, Massive MIMO reveals many new and challenging problems. From a theoretical and research standpoint, coherently measuring and accurately modelling the channel are crucially important, and for real-time system implementations, hundreds of data streams need to be managed and processed, ensuring an acceptable turnaround time (latency) from channel estimation to Downlink (DL) precoding. The Time Division Duplex (TDD) Massive MIMO architecture is also likely to require a new network protocol design to address the channel reciprocity issue, which requires periodical updates of the calibration coefficients [4]. This design is expected to be dependent on deployment scenario (e.g. indoor or cellular).

Prototyping work for various aspects of Massive MIMO technology is ongoing in around the world. The ArgosV2 testbed [5] was developed at Rice University and aims to demonstrate the feasibility of the Massive MIMO concept by using 96 operating antennas to achieve 16 simultaneous streams. Titan Massive MIMO [6] claims to provide a distributed solution for the baseband processing with support for a large number of RF chains through a two-layer linear processing method. Simulations of the Titan system showed a good trade-off between performance and system complexity. The Ngara demonstrator in Australia [7] uses low-cost hardware and was reported to have achieved a spectral efficiency of 67.26 bps/Hz (18 users in a 14MHz bandwidth) in a static lab environment at 638MHz using Frequency Division Duplex (FDD). The Ngara demonstration used offline-calculated channel estimation for DL precoding, and throughput was not measured in real-time. Lund University, also in collaboration with National Instruments (NI), have published numerous papers, for example [8], [9], describing their co-located Massive MIMO testbed.

In this paper, we present a sub-6GHz Massive MIMO research platform that is under development in the Communication Systems & Networks Research Group at the University of Bristol [10]. The platform is being built as part of the wider "Bristol Is Open" (BIO) programme [11]. The system is being developed in collaboration with NI and the University of Lund. The main building blocks and system architecture of the testbed are covered in [12]. It is worth noting that the common virtue of Lund's testbed and ours lies in the modular and scalable design using commercially available hardware. Nevertheless, one major advantage of our testbed lies in our ability to deploy the system in a distributed manner. A brief description of the unique features of the Bristol testbed is given in [13]. At a top-level, the Bristol BS prototype consists of 64 NI Universal Software Radio Peripheral Reconfigurable Input and Output (USRP RIO) software defined radios (SDRs), each capable of supporting 2x2 MIMO. 128 dipole antennas are deployed at the Base Station (BS), whilst 6 USRP RIOs act as 12 single-antenna UEs. This paper reports the first measurement campaign conducted using this testbed in a large indoor venue, which

differs from current cellular deployments where the massive BS is placed outdoors. Real-time simultaneous channel measurements were conducted at all 112 active BS antenna ports at 3.51GHz for 12 transmitting UEs over a 20MHz bandwidth. To the best of the authors' knowledge this is the first time real-time simultaneous MIMO channel measurements have been reported and analysed at massive scale. Furthermore we also record the temporal channel characteristics. The system operates in a TDD fashion with an LTE-like Physical Layer framework that, when fully deployed, enables real-time throughput measurements on the Uplink (UL) and DL according to a user-defined frame schedule. This trial also sets a world record of real-time uplink uncoded spectral efficiency of 79.4bps/Hz with a 5.5m-long linear array [10].

In this paper, we will focus on using our channel measurements to quantify the theoretic maximum downlink throughput achievable in such indoor environment. In TDD operation, the UL channel estimation is used for downlink channel precoding. Using eigen-beamforming (EBF), both the achievable capacities and the number of data streams that can be supported for different scenarios are investigated. The gain that is realistically obtainable by scaling up the number of BS antennas has also been investigated. Additionally, performance is discussed with relation to the channel characteristics, user resolvability, and both the physical size and geometry of the array.

The remainder of this paper is organised as follows: Section II presents testbed overview, the channel estimation procedure and antenna array configurations. Section III describes the experimental environment and various test scenarios, along with the system-level simulator used for throughput prediction. Results for the aggregated user spectral efficiency (SE) and orthogonality metrics are given in Section IV. Finally, Section V summarises the performance gains of Massive MIMO and outlines future measurement plans.

II. Testbed Overview

A. Top-level Capability and Modes of Operation

The Bristol Is Open (BIO) testbed is a real-time 128-antenna Massive MIMO platform that serves up to 12 spatial streams. It is capable of supporting the following MIMO signal processing algorithms: Minimum Mean Square Error (MMSE), Zero-Forcing (ZF) & Maximal Ratio Combining (MRC) detection, and ZF & Maximum Ratio Transmission (MRT) precoding on the DL. For this experiment, only the estimated UL channel data was utilised and the following section focuses on how this was achieved.

B. Channel Estimation

UL channel estimation is scheduled to occur at the beginning of every time slot using the default frame schedule, which is closely matched to Time Division (TD) LTE standard and shown on the right-hand side in Fig. 1. This schedule can be customised if necessary at the OFDM symbol level. During our measurement, we assigned the OFDM symbols after the pilot to be UL data only. For the UL pilot symbol, each UE transmits one QPSK pilot per 12-subcarrier resource block to ensure pilot orthogonality. Over the 1200 data subcarriers present, this equates to 100 pilots per stream spread across the

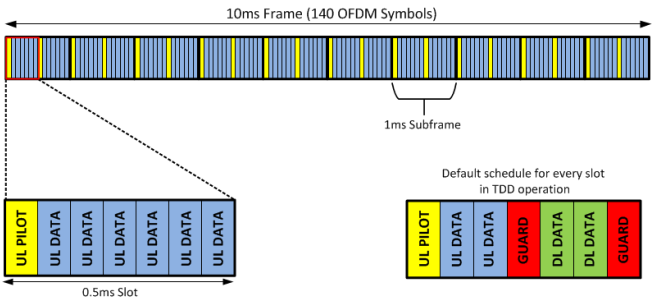

Fig. 1. UE-defined and default frame scheudle

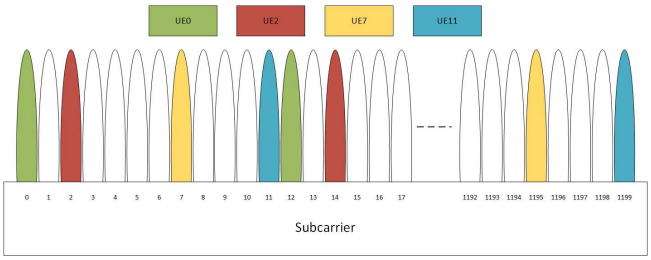

Fig. 2. Allocation of pilots for each user across 1200 subcarriers.

band in 12-subcarrier intervals. Hence, we assume a minimum coherence bandwidth of 180kHz (15kHz subcarrier spacing). An illustration of this subcarrier based pilot allocation for a few UEs is shown in Fig. 2.

Whilst the pilot processing occurs on the FPGA hardware in order to meet the required real-time rates, the raw subcarriers received for one UL Pilot symbol per frame (10ms) are sent to the host computer via a DMA (Direct Memory Access) FIFO for floating point processing. The $\boldsymbol{H}_l^{raw}$ channel estimate for each subcarrier l are formed by dividing the received subcarriers by the expected QPSK pilots. We periodically snapshot the channel estimation to a file for offline processing. As the environment was relatively static for these indoor measurements, 100 channel snapshots were written to disk at an interval of approximately one every 200ms.

C. Antenna Elements

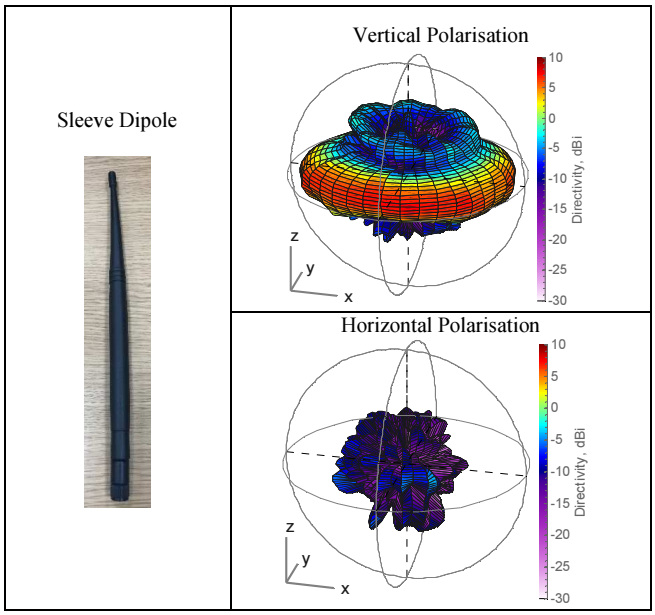

Fig. 3. Measured antenna elements and radiation patterns.

TABLE I. BS & UE ANTENNA ELEMENT STATISTICS

	Percentage Power in each polarisation		Max. Directivity in each polarisation (dBi)	
	Vertical	*Horizontal*	*Vertical*	*Horizontal*
Sleeve Dipole	92%	8%	7.87	-3.77

The BS and UEs use the same sleeve dipole antenna elements shown in Fig. 3 (left). The far-field antenna patterns are shown in the right column for both vertical and horizontal polarisations. Table I lists the percentage of radiated power in the vertical and horizontal polarisations, along with the maximum directivity for each polarisation. The antenna element is heavily vertically polarised. The 3dB beam width is 33º and 360º in the elevation and azimuth planes respectively.

D. BS Array and UE Antenna Configurations

Fig. 4(a) shows the BS antenna array configuration. Two dipole antennas were connected to the front of each USRP (each having 2 transceiver chains), and the spacings between elements are illustrated in the abstracted diagram - Fig. 4(b). Additionally, the black square indicate a subsystem of 14 antenna elements; the red and blue lines enclose active antennas in the 64-antenna and 32-antenna case respectively. The BS array was down-tilted by around 30° to optimise the user's signal to noise ratio (SNR). With a wavelength of 8.6cm at a carrier frequency of 3.51GHz, all the element spacings were large enough to minimise coupling effects.

(a)

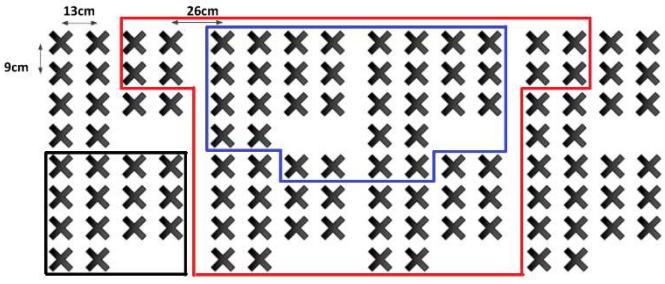

(b)

Fig. 4. BS antenna configurations.

Fig. 5 shows the two UE configurations considered in this paper: a linear array running parallel to the BS array with each UE equidistant (approximately 13cm distance between UE antennas) and a circular array with a diameter of approximately 30cm (smallest antenna spacing was approximately one half of the carrier wavelength).

III. EXPERIMENT OVERVIEW

A. Measuremnt Environment

The measurement campaign was performed in the lower atrium of the Merchant Venturers Building at the University of Bristol (Fig. 6).

Measurements were captured in a large, open indoor venue, with high glass ceilings and stairs leading to an upper level. Measurements were taken after working hours to limit undesirable changes in the propagation environment. Line-of-

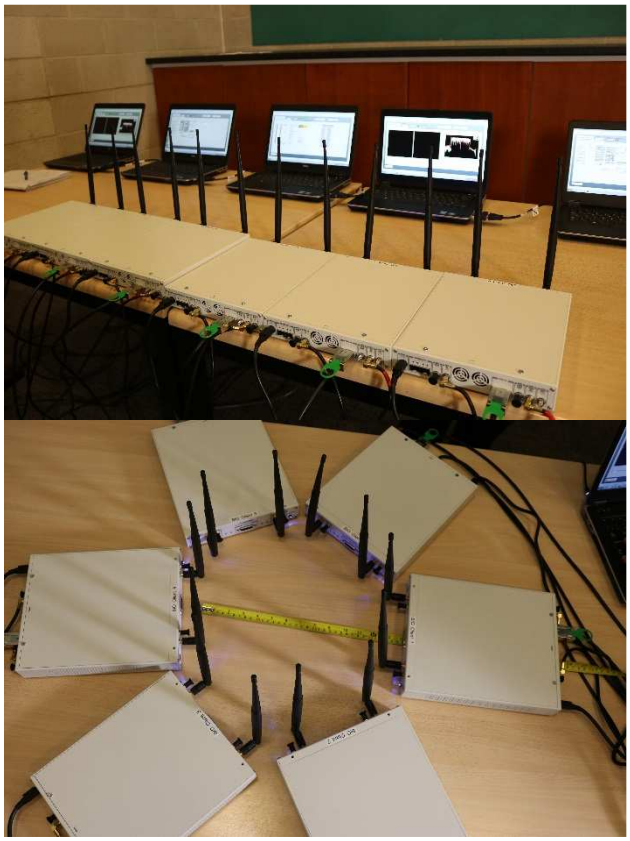

Fig. 5. UE antenna configurations: linear (top) and circular (bottom).

Fig. 6. Measurement environment (view from the BS towards the UEs).

sight (LoS) was always maintained between the BS and the 12 UE elements. The UEs were located 20.8m from the BS. This set-up was particularly useful for understanding user resolvability as the BS antenna number increased.

B. Channel Normalisation

As discussed in the Section II.B, the saved channel coefficients were raw complex numbers calculated by multiplying the received subcarriers by the inverse of the reference pilots. We first normalise the users' channels such that the channel coefficients have unit average energy over all M=112 antenna ports, N=12 users and across all L=100 subcarriers. This was achieved by applying equation (1).

$$\mathbf{H}_{norm,l,t} = \sqrt{\frac{\mathrm{M*N*L}}{\sum_{l=1}^{\mathrm{L}} \|\boldsymbol{H}_l^{raw}\|_F^{\,2}}}\,\boldsymbol{H}_{l,t}^{raw} \qquad (1)$$

where $\boldsymbol{H}_{norm,l,t}$ denotes the normalized channel matrix of size 12×112 at the l^{th} subcarrier and at time instance t. $\| \|_F$ represents the Frobenius-norm of a matrix. This normalisation keeps any differences in channel attenuation between the users, as well as variations over BS antenna elements and frequencies [9].

C. MU Eigen-Beamforming Channel Precoding

We perform singular value decomposition (SVD) of the overall frequency domain channel matrix, $\boldsymbol{H}_{norm,l,t}$, and perform Eigen-Beamforming.

$$\boldsymbol{H}_{norm,l,t} = \boldsymbol{U}_{l,t}\boldsymbol{S}_{l,t}\boldsymbol{V}_{l,t}{}^{H} \qquad (2)$$

at the l^{th} subcarrier and at time instance t, $\boldsymbol{U}_{l,t}$ and $\boldsymbol{V}_{l,t}$ represent the left and right unitary matrices, and $\boldsymbol{S}_{l,t}$ is a diagonal matrix of singular values arranged in decreasing order. Since each stream is pair-wise orthogonal the inter-stream-interference is zero and the effective SINR of the i^{th} stream is equal to its SNR, which is calculated as shown below,

$$SINR_i = P_{tx,i} * \frac{|\lambda_i|^2}{|\sigma_0|^2} \qquad (3)$$

where λ_i represents the i^{th} singular value and σ_0 is the standard deviation of the noise power. $P_{tx,i}$ denotes the transmit power for the i^{th} data stream. Here we assume the transmit power is equally allocated between the streams, while maintaining a normalised total transmit power of unity irrespective of the number of BS antennas. When increasing the number of transmit antennas, the array gain increases, and we choose to harvest this as improved interference performance and user orthogonality, as well as increased receive SNR at the users through beamforming.

The singular value spread (γ) is defined as the ratio of the largest to the smallest singular values of $\boldsymbol{H}_{norm,l,t}$,

$$\gamma = \frac{\max_i\{\lambda_i\}}{\min_i\{\lambda_i\}}, \qquad (4)$$

γ is then averaged across all the subcarriers. It is often used as an indicator of user orthogonality in MU-MIMO scenarios. Cumulative Distribution Function (CDF) plots for γ are provided in section IV along with empirical observations for all channel captures.

D. RBIR Abstraction Simulator

To perform system-level analysis in a computationally efficient and scalable manner, an LTE-like PHY layer abstraction technique, known as RBIR, was used to predict the packet error rate (PER) from the effective SINR for a given channel realisation across the allocated OFDM subcarriers. This technique is fully described in [14] and the references therein, and was also used in [15] and [16]. Without sacrificing accuracy, the runtime of the RBIR simulations is many hundreds of times faster than full bit-level simulation.

Selection of the optimal Modulation and Coding Scheme (MCS) is performed per data stream based on the mode that achieves the highest link throughput conditioned on the PER remaining below 10%. In our system simulations, optimal Adaptive Modulation and Coding (AMC) is achieved through an exhaustive search; details of the algorithm can be found in [16], [17]. The expected throughput is then calculated using the PER and the peak error-free data rate (for the supported number of spatial streams and the chosen MCS mode). The expected throughput is averaged over 100 channel captures.

It is important to note that the EBF performance evaluated here is the capacity for the maximum number of parallel data streams that could be supported under the given channel condition whilst satisfying the power and PER constraints mentioned previously. Therefore, the throughput can be considered to represent the theoretical upper bound of the captured channel for this system.

IV. Theoretic DL Throughput Performance

The measurements presented here target an isolated deployment of a Massive MU-MIMO system serving 12 clients. Fig. 7 shows the spectral efficiency of various configurations as the average user SNR increases from 0dB to 30dB.

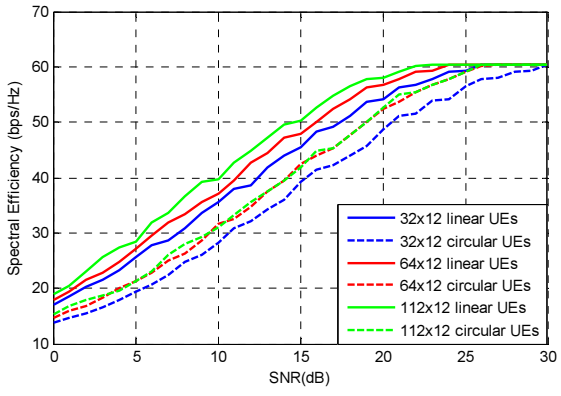

Fig. 7. Spectral efficiency for average user SNR ranging from 0dB to 30dB for various settings.

Although theoretic SNR values can be very high, in practice the Error Vector Magnitude (EVM) specifications limits the maximum SNR practically observed at the UE. For this study, we assumed a maximum average SNR of 30dB at the UE (which translates to an EVM of around 3%). The highest MCS mode is 256QAM with ¾ rate coding, therefore the peak system throughput is a little over 1.2Gbps for 12

users operating over a 20MHz bandwidth. This translates to a peak spectral efficiency (SE) of approximately 60bps/Hz, which represents the upper bound for all our antenna scenarios. It is worth highlighting that our throughput upper bound is specific to the 12-stream operation used in our measurements. As more streams (users) are added, the theoretic upper-bound throughput scales linearly. More streams can be supported if the matrix channel provides good user orthogonality (although this is a trade-off against array and diversity gain).

Before the SE saturates, it increases almost linearly with SNR, indicating good Eigen-structure in the channel matrix and no large power differences between the users due to the LoS environment [18]. Since there was limited movement during the measurements, the channel conditions stayed relatively static between captures; hence the stable estimation of throughput. When the users are spaced apart in a straight line (the 'linear' case), the SE is always better than when the users are arranged in a circle (the 'circular' case). In the latter arrangement the elements are closer to one another. It is interesting to see that *SE_linear* with just 32 antennas outperforms *SE_circular* with 112 antennas by 3bps/Hz at 15dB SNR. The circular placement is particularly difficult for the BS to spatially distinguish the users' signals when a strong LoS is present.

Table II summarises the average SE across the entire SNR range and over all 100 channel captures. A noteworthy observation is that increasing the antenna number from 64 to 112 brings almost no SE improvement in the 'circular' configuration. It is clear in Fig. 2(b) that the aperture of the array is the same in the vertical domain. In this paper, the array aperture refers to the dimension of the array. It is safe to conclude that increasing the number of horizontal elements in this case does not bring any improvement in angular resolvability, and the scattering clusters in the horizontal plane are not rich enough to allow more DoF to be exploited. In the 'linear' configuration, users are sufficiently further apart, i.e. larger than the angular resolution of the BS, and are thus easier to spatially separate. This provides for greater diversity and the possibility of more DoFs in the system. As a result, a large array aperture with an extended vision range of the environment can be exploited to enhance capacity.

TABLE II. AVERAGE SE FOR VARIOUS SETTINGS

Avg. SE (bps/Hz)	32x12 circular	32x12 linear	64x12 circular	64x12 linear	112x12 circular	112x12 linear
EBF	38.0	43.1	40.5	44.9	40.7	46.5

From Fig. 8 we are able to understand how often each rank gets supported over the captured channel as well as the valid range of SNR values. It is worth noting that the number of streams shown here corresponds to the maximum supported number of streams satisfying the PER<10% constraint, which does not necessarily mean the optimal mode of operation. It is impressive that more than 7 data streams can be supported in all of the scenarios. For both UE configurations, full rank is supported almost 80% of the time; this again implies a good Eigen-structure in the channel matrix. The 32-element cases still offer a reasonably high probability of full-rank operation, only 10% short of their 112-element counterparts.

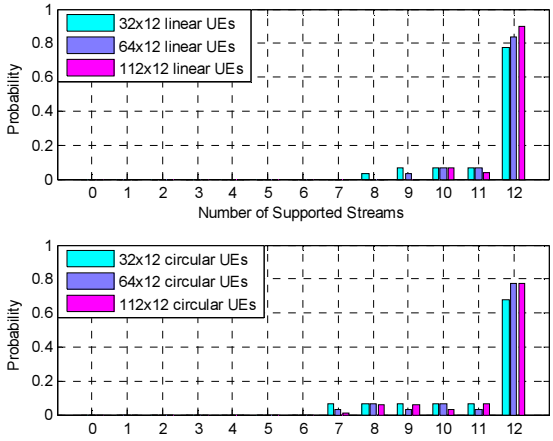

Fig. 8. Histogram of maximum supported number of streams.

Good user orthogonality is a prerequisite in realising the full benefit of spatially multiplexing multiple users in the same time-frequency resource. One simple way to evaluate joint orthogonality of all users is the singular value spread (SVS) of the normalized propagation matrix. Fig. 9 illustrates the CDF plot of the SVS for each scenario and antenna configuration used. In the linear user configuration, the median of the SVS reduces from 11.9 dB to 9.3 dB, as the number of antennas increases from 32 to 112. This observation is very closely matched to the channel sounder measurement reported in [9]. In the 'circular' configuration, a similar drop from 14.3dB to 12.2dB in the median value of the SVS can be seen. The median SVS of an independent and identically distributed (i.i.d.) Rayleigh channel with 112 antennas is below 5dB, which is significantly smaller than our measured results. This indicates degraded channel orthogonality in the measured channels (compared to i.i.d Rayleigh), due to co-location of the users and strong LoS conditions in this scenario. Despite this, the SVS still decreases as the antenna number increases. This implies that the spatial separation of the co-located users can be greatly improved by using a large number of antennas at the BS. It is observed that there is a reduction in the average SEs when there are larger singular value spreads in the measured channels. It is also important to point out that the CDF curves are very stable and have no substantial variances, which is the direct result of the LoS condition, since there is minimal power variation across the antennas.

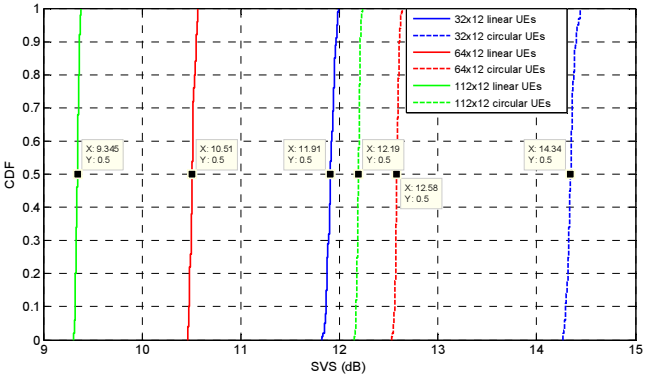

Fig. 9. CDF plot of the singular value spreads and the median values for various settings.

V. CONCLUSIONS

This paper has presented the first set of channel measurements from the BIO Massive MIMO testbed as well as upper bound capacity predictions for a variety of array and client scenarios. Most importantly, we have presented the first real-time instantaneous channel measurements for 112 antenna ports at the BS and 12 single element UEs. From the measured indoor channel data, we have quantified the theoretic system level performance of our Massive MIMO system assuming classic EBF precoding. The benefit of scaling up the number of BS antennas is clearly visible in terms of the average spectral efficiency and resolvability of the users. We also showed that the smaller the singular value spread of the normalised channel matrix, the larger the average spectral efficiency, which strengthens the correlation between SE and good user orthogonality. Future measurement campaigns will include channel measurements for NLoS scenarios, in dynamic environments, real-time UL and DL throughput measurements and a more rigorous investigation of the impact of BS array aperture on system performance.

ACKNOWLEDGMENTS

The authors wish to thank Bristol Is Open (BIO) for access to the hardware facility. They also acknowledge the financial support of the EPSRC CDT in Communications (EP/I028153/1), NEC and National Instruments. Contributions from the University of Lund (Professors Edfors, Tufvesson and their research team) alongside that from National Instruments (Nikhil Kundargi and Karl Nieman) in the on-going development of the Massive MIMO Reference Design are most gratefully acknowledged. The authors would also like to acknowledge support from Nokia Networks (US).

REFERENCES

[1] J. Hoydis, S. Brink and M. Debbah, "Massive MIMO in the UL/DL of Cellular Networks: How Many Antennas Do We Need?," *IEEE Journal on Selected Areas in Communications,* Feb 2013.

[2] T. L. Marzetta, "Noncooperative cellular wireless with unlimited numbers of base station antennas," *IEEE Trans. Wireless Commun.,* vol. 9, no. 11, pp. 3590 -3600, 2010.

[3] E. G. Larsson, O. Edfors, F. Tufvesson and T. L. Marzetta, "Massive MIMO For Next Generation Wireless Systems," *IEEE Communications Magazine,* pp. 186-195, 2014.

[4] F. Rusek, D. Persson, B. Lau, E. Larsson, T. Marzetta, O. Edfors and F. Tufvesson, "Scaling up MIMO: Opportunities and Challenges with Very Large Arrays," *IEEE Signal Processing Magzine,* Jan 2013.

[5] C. Shepard, H. Yu and L. Zhong, "ArgosV2: A Flexible Many-Antenna Research Platform," in *MobiCom*, Miami, US, 2013.

[6] S. Roy, "Two-Layer Linear Processing for Massive MIMO on the TitanMIMO Platform," 27 Jan 2015. [Online].

[7] H. Suzuki and e. al, "Highly Spectrally Efficient Ngara Rural Wireless Broadband Access Demonstrator," in *International Symposium on Communications and Information Technologies (ISCIT)*, 2012.

[8] J. Vieira and e. al, "A flexible 100-antenna testbed for Massive MIMO," in *Globecom 2014 Workshop - Massive MIMO: From Theory to Practice*, 2014.

[9] X. Gao, O. Edfors, F. Rusek and a. F. Tufvesson, "Massive MIMO Performance Evaluation Based on Measured Propagation Data," *IEEE Trans on Wireless Communications,* vol. 14, no. NO. 7, 2015.

[10] "Bristol and Lund set a new world record in 5G wireless spectrum efficiency," Univeristy of Bristol, [Online]. Available: http://www.bristol.ac.uk/news/2016/march/massive-mimo.html. [Accessed 25th March 2016].

[11] "Bristol Is Open," 2015. [Online]. Available: http://www.bristolisopen.com.

[12] E. Luther, "5G Massive MIMO Testbed: From Theory to Reality," National Instruments, 21 Sep 2015. [Online]. Available: http://www.ni.com/white-paper/52382/en/.

[13] P.Harris, S.Zhang, A.Nix, M.Beach, S.Armour and A.Doufexi, "A Distributed Massive MIMO Testbed to assess Real-World Performance & Feasibility," in *IEEE VTC-Spring*, 2015.

[14] D. Halls, A. Nix and M. Beach, "System level evaluation of UL and DL interference in OFDMA mobile broadband networks," in *IEEE Wireless Communications and Networking Conference*, 2011.

[15] S.Zhang, D. Kong, E. Mellios, G. Hilton, A. Nix, T. Thomas and A. Ghosh, "Impact of BS Antenna Number and Array Geometry on Single-User LTE-A Data Throughputs in Realistic Macro and Pico Cellular Environments," in *IEEE Wireless Communications and Networking Conference*, New Orleans, US, 2015.

[16] S. Zhang, D. Kong, E. Mellios, A. Doufexi and a. A. Nix, "Comparing Theoretic Single-User and Multi-User Full-Dimension MIMO Data Throughputs in Realistic City-Wide LTE-A Deployments," in *IEEE Globecom*, San Diego, US, 2015.

[17] Y. Bian, A. Nix, E. Tameh and a. J. McGeehan, "MIMO–OFDM WLAN Architectures, Area Coverage, and Link Adaptation for Urban Hotspots," *IEEE Trans. Veh. Tech,* vol. 57, no. 4, 2008.

[18] A. O. Martinez, E. D. Carvalho and J. Ø. Nielsen, "Towards Very Large Aperture Massive MIMO," in *IEEE GLOBECOM*, 2014.